


Article

# Design and Performance Analysis for the Low-Power Holding Mechanism of the All-Electric Subsea Gate Valve Actuator

Honghai Wang <sup>1</sup>, Peng Jia <sup>1,\*</sup>, Liquan Wang <sup>1</sup>, Feihong Yun <sup>1</sup>, Gang Wang <sup>1</sup> , Aiguo Zhang <sup>2</sup>, Min Xu <sup>2</sup> and Xiangyu Wang <sup>1</sup>

<sup>1</sup> College of Mechanical and Electrical Engineering, Harbin Engineering University, Harbin 150001, China; wanghonghai920303@163.com (H.W.); wangliquan@hrbeu.edu.cn (L.W.); yunfeihong@hrbeu.edu.cn (F.Y.); wanggang@hrbeu.edu.cn (G.W.); wangxiangyu325@126.com (X.W.)

<sup>2</sup> HEU Qingdao Ship Science And Technology Co., Ltd., Qingdao 266400, China; zhangaiguo@hrbeu.edu.cn (A.Z.); xumin880722@163.com (M.X.)

\* Correspondence: jiapeng@hrbeu.edu.cn

Received: 15 July 2020; Accepted: 2 September 2020; Published: 3 September 2020



**Abstract:** The all-electric subsea gate valve actuator is one of the critical components of the all-electric subsea production control system. To bridge the gap of the low-power holding mechanism in the all-electric subsea gate valve actuator of the subsea production system, minimize the power consumption and cable number for control and improve the open-position keeping performance of all-electric subsea gate valve actuator, this paper proposed a novel low-power holding mechanism for the all-electric subsea gate valve actuator which can be applied to all-electric subsea gate valve actuators with various valve sizes and process pressure ratings. The proposed low-power holding mechanism uses an electromagnet as a driving element, combines the spiral transmission and the cam-like transmission, and only requires a holding force of approximately 2–7% of the maximum load of the closing spring to keep the valve open. The proposed low-power holding mechanism converts the axial force of the closing spring into the circumferential force, which substantially reduces the output force required for the driving element of the low-power holding mechanism and the number of the actuator's control cables. Analytic models are created for the lockable maximum load of the closing spring and the permissible stroke of the locking tab with regard to the design variables. The parameter effects and the corresponding sensitivities are discussed by numerical analysis. The design parameters and the lockable maximum load of the closing spring of the low-power holding mechanism are obtained.

**Keywords:** all-electric subsea production control system; all-electric subsea gate valve actuator; low-power holding mechanism; configuration research; performance analysis

## 1. Introduction

Late in the last century, in order to meet the needs of deep-water gas and oil exploitation, subsea equipment suppliers began to develop and improve the all-electric subsea control technology [1]. The all-electric Subsea Production Control System (AE), a leading-edge and breakthrough technology, which didn't need hydraulic fluid and was driven completely by electric power, was proposed and developed [2]. The key benefits of the AE system compared to the conventional Multiple Electric-Hydraulic Control System (MEH) are as follows [3–10]: the simplified system structure, enhanced control performance, improved system reliability and availability, increased the oil recovery factor and environmental friendliness. Furthermore, the advantages of AE system also include: the decreased power consumption [11,12], reduced Capital expenditure(CAPEX) and Operating

expenditure(OPEX) [13–16], strengthened intelligence [17,18]. Therefore, with the improvement of key techniques of the AE system, the AE system will replace the MEH system as a trend in the future [19–21].

The all-electric subsea gate valve actuator is one of the critical components of the AE system [6,7], which is used to open and close the production gate valve for the subsea Xmas tree. Its performance directly affects the reliability and safety of the AE system. Similar to the traditional hydraulic-driven subsea gate valve actuator, in the opening and closing processes of the valve, the all-electric subsea gate valve actuator is required to have a failsafe close ability, Remotely Operated Vehicle(ROV) override function, subsea ambient pressure compensation and valve position indication [22,23]. The all-electric subsea gate valve actuator uses the motor as the actuation unit, and the service life cycle of the motor is lower than that of the hydraulic cylinder. Therefore, to ensure the high reliability of the actuator, the actuation device should be designed with regard to redundancy [24]. In addition, the subsea gate valve is a normally open valve. When the valve is opened, the power system needs to resist the resilience of the failsafe closing mechanism, which consumes a lot of energy in long term operation [25]. Thus, to reduce the energy consumption, the low-power holding mechanism is required for the all-electric subsea gate valve actuator to ensure that the valve remains open with small power consumption.

The research and development of all-electric subsea gate valve actuators are in the early phase. A few oil companies like Cameron and FMC have carried out relevant research on it. Cameron's all-electric subsea gate valve actuator realized the opening and closing operation of the subsea gate valve through a high-power "drive" motor, and was equipped with a low-power "clutch" motor to ensure that the valve remained open by means of a friction-based mechanism. Further, a closing spring was used as the failsafe close solution [6,7]. FMC's all-electric subsea gate valve actuator powered the built-in motion control system via locally stored power from rechargeable batteries and capacitors to open and close the subsea gate valve and was equipped with the ROV interface. No springs were required to move a valve to a failsafe position [8,11]. At present, the all-electric subsea gate valves actuator of each oil company are still in the initial application stage, and the key technology of has not yet matured. Winther-Larsen [26] developed a functional design specification for the all-electric subsea gate valve actuator and proposed a design for an all-electric subsea gate valve actuator, as well as the motor control system layout based on the specification. Jon Berven [27] discussed failsafe solutions of the all-electric subsea gate valve actuator and created the calculation method of the peak load and the applied torque of the actuator. Wang [24] proposed the multi-motor parallel redundant method to drive the valve and designed the structure of an all-electric subsea valve actuator. Xiao [28] developed a subsea all-electric Christmas tree gate valve actuator and analyzed the sealing process of the gate valve. Liu [25] proposed a new pressure compensation all-electric control gate valve and actuator integrated structure, which substantially reduced the high-pressure hydraulic resistance during valve closure.

According to the above analysis, it is obvious that some designs and researches have been done for the all-electric subsea gate valve actuator. However, most of the existing researches on the all-electric subsea gate valve actuator do not concentrate on the low-power holding mechanism, which was the unique composition of the all-electric subsea gate valve actuator. Therefore, a low-power holding mechanism of the all-electric subsea gate valve actuator is proposed in this paper, which uses an electromagnet as a driving element and combines spiral transmission and cam-like transmission, the corresponding mechanical and kinematic models are also established, respectively. The analytic expression of the relation is derived, respectively, for the lockable maximum load of the closing spring and the permissible stroke of the locking tab with regard to the design variables. The parameter effects and the corresponding sensitivities are analyzed as well. The lockable maximum load of the closing spring and the design parameters of the low-power holding mechanism are obtained.

This present work is aimed at developing a novel and feasible low-power holding mechanism of the all-electric subsea gate valve actuator, which can minimize the power consumption and cable

number for control and improve the open-position keeping performance of an all-electric subsea gate valve actuator, only requiring a holding force of approximately 2%~7% of the maximum load of the closing spring to keep the valve open and with the ability to be applied to all-electric subsea gate valve actuators with various valve sizes and process pressure ratings, to bridge the gap of the low-power holding mechanism in the all-electric subsea gate valve actuator of the subsea production system.

The rest of the paper is organized as follows: Section 2 briefly introduces the working process of the all-electric subsea gate valve actuator proposed, followed by a full presentation of the configuration, work principle and advantage of the proposed failsafe closing and low-power holding mechanism. Section 3 presents the mechanical and kinematic models. In Section 4, the detailed discussion of the parameter effects and sensitivity analysis is performed based on the established model and results. Finally, conclusions are given in Section 5.

## 2. Research on the Configuration of Failsafe Closing and Low-Power Holding Mechanism

Based on the function of the all-electric subsea gate valve actuator, a configuration of the all-electric subsea gate valve actuator is proposed in this paper, as shown in Figure 1, wherein the structure mainly includes the subsea gate valve assembly, failsafe closing and low-power holding mechanism, subsea ambient pressure compensating mechanism, screw drive mechanism, multi-motor redundant driving mechanism, valve position indicating mechanism and ROV interface. During the valve opening process, multi-motor redundant driving mechanism or ROV drives the valve stem and gate downward to open the subsea gate valve through the screw drive mechanism. After the subsea gate valve is fully opened, the low-power holding mechanism locks the failsafe closing mechanism to ensure that the valve remains open with the minimum power consumption. When the all-electric subsea production control system breaks down, the low-power holding mechanism and multi-motor redundant driving mechanism are power-off, the failsafe closing mechanism drives the valve stem and gate upward to realize the emergency failure close.

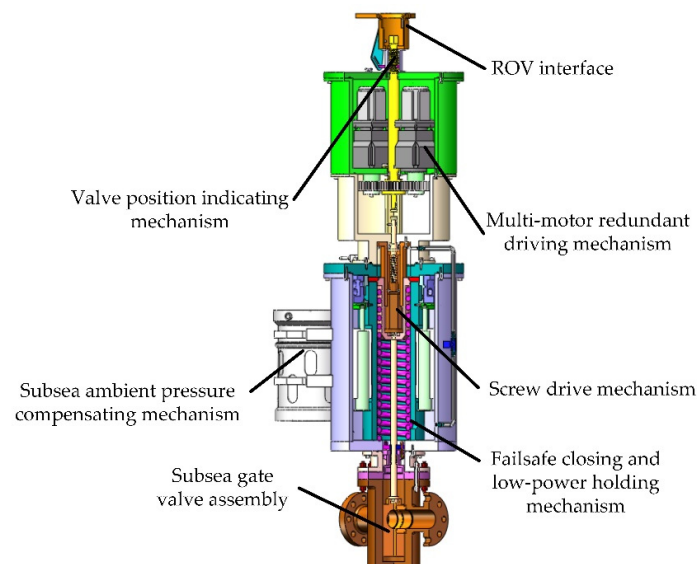


**Figure 1.** Schematic diagram of the all-electric subsea gate valve actuator.

Failsafe closing mechanisms of the subsea valve include the mechanical failsafe closing mechanism and Uninterrupted Power System (UPS) failsafe closing mechanism [29,30]. As the service life cycle of the subsea Xmas tree or manifold is usually around 20 years, long term continuous power supply makes the UPS failsafe closing mechanism unpractical. The mechanical failsafe closing mechanism is most commonly used for this purpose. In the application of the mechanical failsafe closing mechanism for a subsea valve actuator, the spring-type configuration is reliable and widely used [4,25]. However, the force of the closing spring needs to be big enough to oppose the high-pressure fluid in the valve

when a failure close occurs. So when the valve is opened, the power system needs to resist the large spring forces, which consume a lot of energy [25]. Thus, the low-power holding mechanism also needed to be designed in the actuator of this paper. In addition, a single Electric Subsea Control Module (ESCM) is claimed to control up to 32 functional groups [6]. However, a single ESCM can control up to 16 functional groups including sensors in an engineering application [12], which puts forward requirements for the number of the actuator's control cables.

Based on the above analysis, the low-power holding mechanism is proposed in this paper, as shown in Figure 2, in which a spiral groove is machined inside the locking ring sleeve; a thread and four cam-like notches are machined outside the locking ring and inside the bottom, respectively. Four locking tabs are adopted due to the higher symmetry and stability of this configuration, compared with the design of two locking tabs. Furthermore, the requirements of this configuration for the size of the locking ring are moderate, because each locking tab needs a cam-like notch of the locking ring. The higher the number of locking tabs, the higher the number of cam-like notches necessary, which leads the size of the locking ring being easily unable to meet the requirements. Thus, the configuration of four locking tabs has advantages in realizing product function, improving product performance and meeting design constraints.

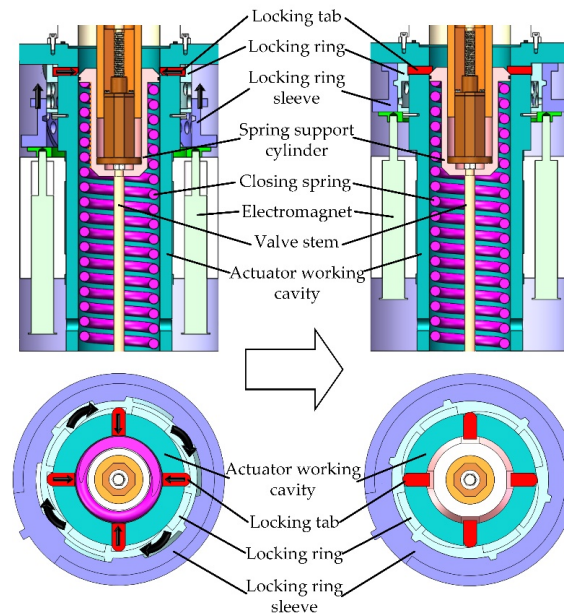


**Figure 2.** The locking and holding process of the low-power holding mechanism.

The locking and holding process of the low-power holding mechanism is shown in Figure 2. The driving mechanism pushes the spring support cylinder against the closing spring until the valve is fully opened, at which point the closing spring is at the limit, and the electromagnets are energized and push the locking ring sleeve upward. The locking ring sleeve drives the locking ring to rotate forward through the spiral groove. Meanwhile, the locking ring drives locking tabs to move inward through the cam-like notch. The locking process of the low-power holding mechanism is completed when the locking tabs fully enter the actuator working cavity and make contact with the slope of the spring support cylinder to block the cylinder moving back. After the locking process, the holding process of the low-power holding mechanism is started. In the holding process, the locking tab and the spring support cylinder constrain each other, and the position of the locking tab is restricted by the locking ring, to ensure that the valve remains open with the minimum power consumption.

When a valve fail-close occurs, the electromagnets are de-energized, thereby the position of the locking tab is not restricted by the locking ring. The unlocking process is opposite to the locking process, and the closing spring force is the driving force for the unlocking process. The closing spring drives the

locking tabs to move outward through the slope of the spring support cylinder. Meanwhile, the locking tabs drive the locking ring to rotate backward through the cam-like notch surface, and the locking ring pushes the locking ring sleeve downward through the spiral groove. The unlocking process is completed when the locking tab and the spring support cylinder are separated. After the unlocking process, the closing spring continues to release rapidly and drives the spring support cylinder and the valve stem upward until the valve is fully closed.

The proposed low-power holding mechanism converts the axial force of the closing spring into the circumferential force by the spiral groove and the cam-like notches, which substantially reduces the output force required for the driving element of the low-power holding mechanism and increases the feasibility and reliability of the holding mechanism. In addition, different from the form of Cameron's "clutch" motor, the proposed low-power holding mechanism is driven by the electromagnet, which effectively reduces the number of the actuator's control cables.

When a fail-close occurs, the maximum load produced by the high-pressure fluid which the all-electric subsea gate valve actuator can oppose depends on the force of the closing spring. According to the configuration of the low-power holding mechanism, the maximum load of the closing spring is related to the size of the low-power holding mechanism. However, the permissible stroke of the locking tab also depends on the size of the low-power holding mechanism and needs to be larger than the given working stroke, which will form a constraint for the optimization of the locking and holding ability of the low-power holding mechanism. Thus, it is necessary to analyze the mechanical and kinematic models of the low-power holding mechanism in detail.

### 3. Mechanical Model and Kinematic Analysis of the Low-Power Holding Mechanism

#### 3.1. Mechanical Model of the Low-Power Holding Mechanism

The low-power holding mechanism adopts four locking tabs to share the maximum load of the closing spring. Figure 3 shows the force analysis of the spring support cylinder and single locking tab in the holding process, in which  $F_{m1}/4$  is the maximum load of the closing spring shared by the single locking tab,  $R_{16}$  and  $R_{61}$  are the interactive force between the spring support cylinder and the single locking tab,  $R$  is the radial component force acting on the spring support cylinder by the single locking tab in the symmetrical direction,  $R_{63}$  and  $R_{36}$  are the interactive force between the single locking tab and the actuator working cavity,  $F_r$  and  $F'_r$  are the interactive radial thrust between the single locking tab and the locking ring.

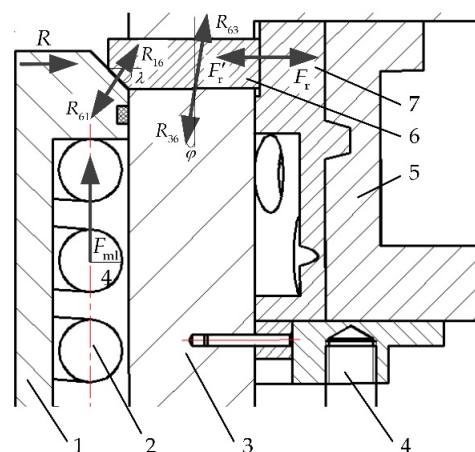


**Figure 3.** The force analysis of the spring support cylinder and single locking tab in the holding process. 1—Spring support cylinder, 2—Closing spring, 3—Actuator working cavity, 4—Electromagnet, 5—Locking ring sleeve, 6—Locking tab, 7—Locking ring.



In the holding process, the spring support cylinder and the single locking tab are in a state of mechanical equilibrium. Figure 4 shows the force diagram of the spring support cylinder and the single locking table as shown in Figure 4a, the relation between  $R_{61}$  and  $F_{m1}$  can be expressed as:

$$R_{61} = \frac{F_{m1}}{4 \cos(\lambda - \varphi)}, \tag{1}$$

where  $\lambda$  is the angle of the slope of the single locking tab;  $\varphi$  is the friction angle;  $F_{m1}$  is the maximum load of the closing spring.

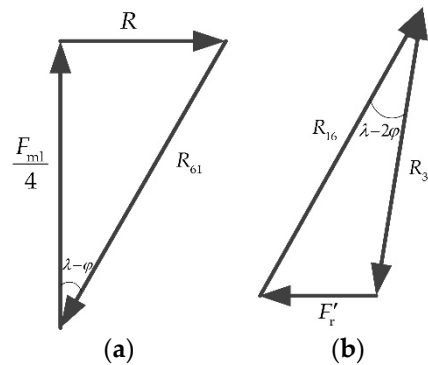


**Figure 4.** The force diagram of (a) the spring support cylinder and (b) the single locking tab.

As shown in Figure 4b, the relation between  $R_{61}$  and  $F_r$  can be given as:

$$\frac{R_{16}}{\sin(90^\circ + \varphi)} = \frac{R_{61}}{\sin(90^\circ + \varphi)} = \frac{F_r'}{\sin(\lambda - 2\varphi)} = \frac{F_r}{\sin(\lambda - 2\varphi)}, \tag{2}$$

Combining Equations (1) and (2), the relation between  $F_r$  and  $F_{m1}$  can be expressed as:

$$F_r = \frac{R_{16} \sin(\lambda - 2\varphi)}{\sin(90^\circ + \varphi)} = \frac{F_{m1} \sin(\lambda - 2\varphi)}{4 \cos(\lambda - \varphi) \cos \varphi}, \tag{3}$$

Figure 5 shows the force diagram of the contact between the single locking tab and the locking ring in the holding process, in which  $R_{67}$  and  $R_{76}$  are the interactive forces between the single locking tab and the locking ring. To facilitate the analysis, the force diagram in Figure 5 is simplified, as shown in Figure 6. This assumes that  $O_1$  is the center of the actuator working cavity;  $O_2$  is the center of the notch of the locking ring;  $O_3$  is the center of the curved surface of the locking tab; C is the contact point between the locking tab and locking ring; the straight line, MN, is the normal direction of the contact point C; S is the starting point of the notch of the locking ring, which is the contact point between the notch and the actuator working cavity; E is the ending point of the notch of the locking ring, which is the intersection of the notch and the line  $O_1O_2$ ;  $\delta$  is the angle of the notch of the locking ring. The angle between  $R_{76}$  and MN is  $\varphi$  since  $R_{76}$  is the resultant force of normal pressure and friction; the direction of  $F_r$  is parallel to  $O_1O_3$ . Because the notch of the locking ring and the actuator working cavity are not concentric, a circumferential force  $F_t$  is introduced at the contact point C, which is not only the resistance to overcome by the low-power retaining mechanism in the holding process, but also the driving force of the backward rotation of the locking ring in the unlocking process. The locking ring rotates around the center  $O_1$  in the locking or unlocking process, so  $F_t$  is perpendicular to the segment  $O_1C$ . Draw line segments begin in the direction of  $F_r$  and  $R_{76}$ , and end at points A and B, respectively, where the segment  $AB \parallel F_t$  and passes through the center  $O_1$ .

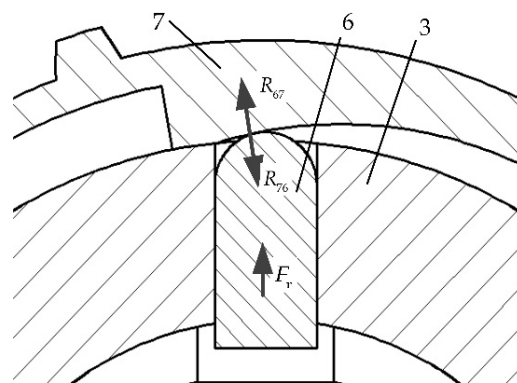


**Figure 5.** The force diagram of the contact between the single locking tab and the locking ring in the holding process. 3—Actuator working cavity, 6—Locking tab, 7—Locking ring.

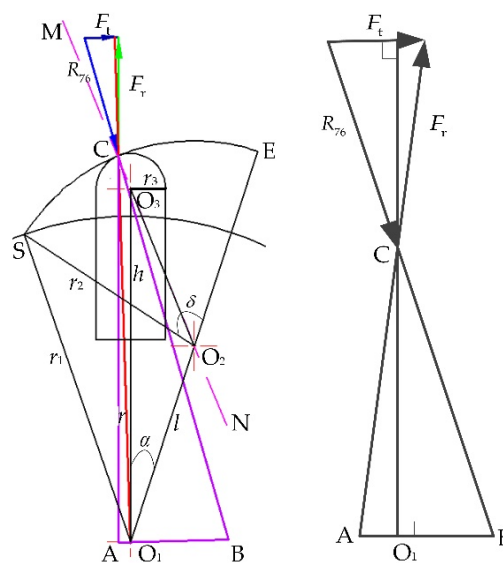


**Figure 6.** The force analysis of the contact between the single locking tab and the locking ring in the holding process.

As shown in Figure 6, the relationship between  $F_t$  and  $F_r$  can be obtained by calculating the relationship between AB and AC. The relevant design parameters of the low-power holding mechanism are listed in Table 1, and the intermediate parameters in the calculation process are listed in Table 2.

**Table 1.** The relevant design parameters of the low-power holding mechanism.

| Parameter Description   | Symbol   |
|---|----------|
| Radius of the actuator working cavity   | $r_1$    |
| Radius of the notch of the locking ring   | $r_2$    |
| Radius of the locking tab   | $r_3$    |
| Center distance between the actuator working cavity and the locking ring notch ( $ O_1O_2 $ ) | $l$      |
| Radial deflection angle of the center of the locking ring notch ( $\angle O_2O_1O_3$ )        | $\alpha$ |

**Table 2.** The intermediate parameters in the calculation process.

| Parameter Description   | Symbol |
|---|--------|
| Center distance between the actuator working cavity and the locking tab ( $ O_1O_3 $ )          | $h$    |
| Distance between the center of the actuator working cavity and the contact point C ( $ O_1C $ ) | $r$    |

In  $\triangle O_1O_2O_3$  and  $\triangle O_1O_3C$ ,  $h, r$  and  $\angle CO_1O_3$  can be obtained, respectively:

$$h^2 = (r_2 - r_3)^2 + l^2 + 2l(r_2 - r_3) \cos \left[ \alpha + \arcsin \left( \frac{l \sin \alpha}{r_2 - r_3} \right) \right], \tag{4}$$

$$r^2 = r_3^2 + h^2 + 2r_3h \cos \left[ \arcsin \left( \frac{l \sin \alpha}{r_2 - r_3} \right) \right] \text{ and} \tag{5}$$

$$\angle CO_1O_3 = \arccos \left( \frac{r^2 + h^2 - r_3^2}{2rh} \right). \tag{6}$$

As  $F_r \parallel O_1O_3$  and  $CO_1 \perp AB$ ,  $\angle CAB$  can be given as:

$$\angle CAB = \frac{\pi}{2} - \angle CO_1O_3 = \frac{\pi}{2} - \arccos \left( \frac{r^2 + h^2 - r_3^2}{2rh} \right). \tag{7}$$

In  $\triangle O_1O_2C$ ,  $\angle O_1CO_2$  can be expressed as:

$$\angle O_1CO_2 = \arccos \left( \frac{r_2^2 + r^2 - l^2}{2r_2r} \right). \tag{8}$$

And  $\angle ACB = \angle O_2CA - \varphi = \angle CO_1O_3 + \angle O_1CO_2 - \varphi$ , so  $\angle ACB$  can be given as:

$$\angle ACB = \arccos \left( \frac{r^2 + h^2 - r_3^2}{2rh} \right) + \arccos \left( \frac{r_2^2 + r^2 - l^2}{2r_2r} \right) - \varphi. \tag{9}$$

Combining Equations (3), (7) and (9), the relation between  $F_t$  and  $F_{ml}$  can be expressed as:

$$F_t = \frac{F_r \sin \angle acb}{\sin \angle abc} = \frac{F_{ml} \sin(\lambda - 2\varphi) \sin \left[ \arccos \left( \frac{r^2 + h^2 - r_3^2}{2rh} \right) + \arccos \left( \frac{r_2^2 + r^2 - l^2}{2r_2r} \right) - \varphi \right]}{4 \cos(\lambda - \varphi) \cos \varphi \cos \left[ \arccos \left( \frac{r_2^2 + r^2 - l^2}{2r_2r} \right) - \varphi \right]}. \tag{10}$$

Since four locking tabs are adopted to share the maximum load of the closing spring, the total circumferential force is  $4F_t$ . Therefore, the total resistance torque between the locking ring and the locking ring sleeve can be expressed as:

$$T = 4F_t \cdot r. \tag{11}$$

Figure 7 shows the force analysis of the locking ring sleeve and the locking ring in the holding process. Assuming that the driving force of the locking ring sleeve is fully sustained by the spiral groove of the locking ring, the actuator working cavity applies no force on the locking ring sleeve. In the holding process, the locking ring tends to rotate backward to drive the locking ring sleeve to move upward. In Figure 7,  $F_D$  is the output force of the electromagnet,  $R_{85}$  is the resultant force of the housing acting on the locking ring sleeve,  $R_{75}$  and  $R_{57}$  are the interactive force between the locking ring sleeve and the locking ring,  $R_{37}$  is the resultant force of the actuator working cavity acting on the locking ring,  $\beta$  is the spiral angle of the locking ring.

As shown in Figure 7, the force to resist the backward rotation of the locking ring is the circumferential resultant force of  $R_{57}$  and  $R_{37}$ , and satisfies:

$$\frac{R_{57} \sin(\beta + 2\varphi)}{\cos \varphi} \cdot R = 4F_t \cdot r, \tag{12}$$

where  $R$  is the spiral radius of the locking ring;  $\beta = \arctan \left( \frac{S}{2\pi R} \right)$ , and  $S$  is the pitch.



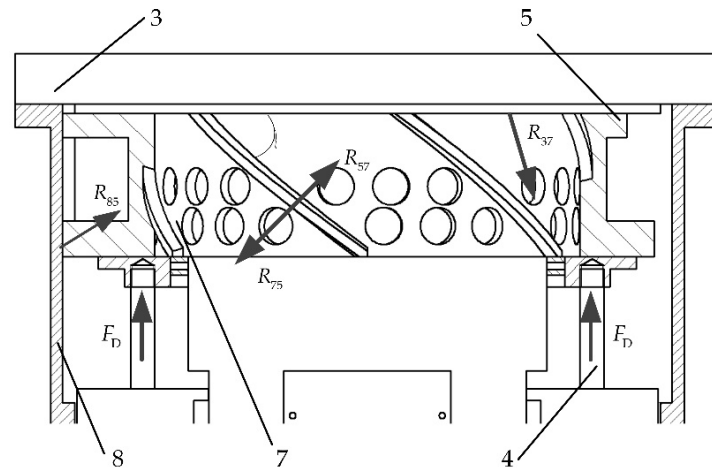


**Figure 7.** The force analysis of the locking ring sleeve and the locking ring in the holding process. 3—Actuator working cavity, 4—Electromagnet, 5—Locking ring sleeve, 7—Locking ring, 8—Housing.

The relation between  $R_{57}$  and  $F_D$  can be expressed as:

$$R_{57} = \frac{F_D \cos \varphi}{\cos(\beta + 2\varphi)}. \tag{13}$$

By substituting Equations (10) and (13) into Equation (12), the lockable maximum load of the closing spring can be obtained, that is:

$$F_{ml} = \frac{F_D \cos(\lambda - \varphi) \cos \varphi \cos \left[ \arccos \left( \frac{r_2^2 + r^2 - l^2}{2r_2r} \right) - \varphi \right] \tan(\beta + 2\varphi) \cdot R}{\sin(\lambda - 2\varphi) \sin \left[ \arccos \left( \frac{r^2 + h^2 - r_3^2}{2rh} \right) + \arccos \left( \frac{r_2^2 + r^2 - l^2}{2r_2r} \right) - \varphi \right] \cdot r}, \tag{14}$$

where

$$h = \left\{ (r_2 - r_3)^2 + l^2 + 2l(r_2 - r_3) \cos \left[ \alpha + \arcsin \left( \frac{l \sin \alpha}{r_2 - r_3} \right) \right] \right\}^{\frac{1}{2}}, \tag{15}$$

$$r = \left\{ r_3^2 + h^2 + 2r_3h \cos \left[ \arcsin \left( \frac{l \sin \alpha}{r_2 - r_3} \right) \right] \right\}^{\frac{1}{2}}. \tag{16}$$

### 3.2. Kinematic Analysis of the Low-Power Holding Mechanism

In the locking or unlocking process, the locking tab moves linearly in the cam-like notch of the locking ring, and the locking ring rotates around the actuator working cavity. Figure 8 shows the relative position between the locking tab and the locking ring in the locking state and unlocking state, respectively. Thus, the constraint condition for the locking tab to complete the locking and unlocking actions can be expressed as:

$$L \leq [L], \tag{17}$$

where  $[L]$  is the permissible stroke of the locking tab;  $L$  is the working stroke of the locking tab.

The permissible stroke of the locking tab depends on the size of the low-power holding mechanism. To facilitate the analysis, the movement of the locking ring and the locking tab is equivalent so that the locking ring remains fixed, while the locking tab not only moves linearly in the notch but also rotates around the actuator working cavity during the locking and unlocking processes. Figure 9 shows the kinematic analysis of the unlocking process of the low-power holding mechanism. Assuming that  $O_{32}$  is the center of the curved surface of the locking tab in an unlocking state;  $O_{31}$  is the intersection of the segment  $O_1O_{32}$  and the arc formed by the rotation of  $O_3$  around  $O_1$ ,  $m$  is the length of the segment

$O_1O_{32}$ . The other symbols have the same values as depicted in Figure 6. The permissible stroke of the locking tab,  $[L]$ , can be expressed as:

$$[L] = m - h. \tag{18}$$

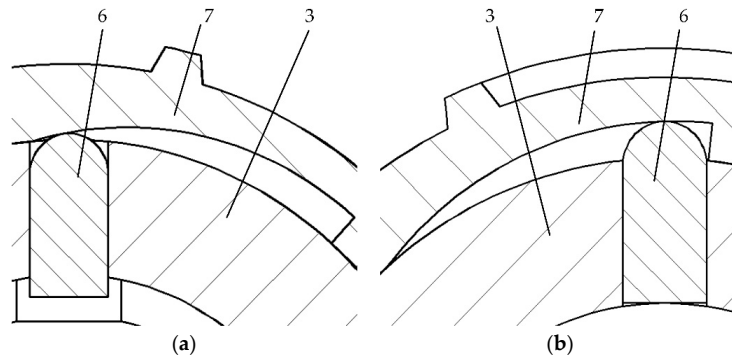


**Figure 8.** The relative position between the locking tab and the locking ring in (a) the locking state, (b) the unlocking state. 3—Actuator working cavity, 6—Locking tab, 7—Locking ring.

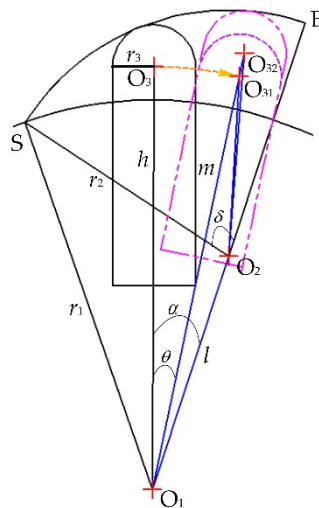


**Figure 9.** The kinematic analysis of the unlocking process of the low-power holding mechanism.

As shown in Figure 9, the rotation angle of the locking ring in the locking or unlocking process  $\theta$  can be given as:

$$\theta = \alpha - \angle O_{32}O_1O_2 = \alpha - \arcsin\left(\frac{r_3}{r_1}\right). \tag{19}$$

So  $\angle O_1O_{32}O_2$  and  $m$  can be expressed as follows, respectively:

$$\angle O_1O_{32}O_2 = \arcsin\left(\frac{l \sin \angle O_{32}O_1O_2}{r_2 - r_3}\right) = \arcsin\left(\frac{lr_3}{r_1(r_2 - r_3)}\right), \tag{20}$$

$$m^2 = (r_2 - r_3)^2 + l^2 + 2l(r_2 - r_3) \cos\left[\arcsin\left(\frac{r_3}{r_1}\right) + \arcsin\left(\frac{lr_3}{r_1(r_2 - r_3)}\right)\right]. \tag{21}$$

By substituting Equations (15) and (21) into Equation (18), the permissible stroke of the locking tab  $[L]$  can be rewritten as:

$$\begin{aligned}
 [L] &= m - h \\
 &= \left\{ (r_2 - r_3)^2 + l^2 + 2l(r_2 - r_3) \cos \left[ \arcsin \left( \frac{r_3}{r_1} \right) + \arcsin \left( \frac{lr_3}{r_1(r_2 - r_3)} \right) \right] \right\}^{\frac{1}{2}} - \left\{ (r_2 - r_3)^2 + l^2 + 2l(r_2 - r_3) \cos \left[ \alpha + \arcsin \left( \frac{l \sin \alpha}{r_2 - r_3} \right) \right] \right\}^{\frac{1}{2}}. \quad (22)
 \end{aligned}$$

### 4. Numerical Analysis and Discussion

#### 4.1. Parameter Effects

The effects of the design parameters in Table 1 on the lockable maximum load of the closing spring  $F_{ml}$  and the permissible stroke of the locking tab  $[L]$ , respectively, are analyzed in this section. Assume that the parameters of the low-power holding mechanism are:  $\lambda = 45^\circ$ ,  $\varphi = 5.7^\circ$ ,  $S = 850$  mm,  $R = 183$  mm,  $F_D = 1600$  N, the required working stroke of the locking tab  $L = 8$  mm, and the design variable ranges are listed in Table 3.

Table 3. The design variable ranges.

| Design Variable Description  | Variable | Variable Range |
|--|----------|----------------|
| Radius of the actuator working cavity  | $r_1$    | 130~150 mm     |
| Radius of the notch of the locking ring  | $r_2$    | 130~150 mm     |
| Radius of the locking tab  | $r_3$    | 10~20 mm       |
| Center distance between the actuator working cavity and the locking ring notch | $l$      | 30~40 mm       |
| Radial deflection angle of the center of the locking ring notch                | $\alpha$ | 35~45°         |

Figure 10 shows the variable effects on the lockable maximum load of the closing spring  $F_{ml}$ .  $F_{ml}$  can be increased by increasing  $r_2$  and/or reducing  $\alpha$ . According to Equations (5), (10) and (11), in the holding process, the resistance arm,  $r$ , increases with the increase in  $r_2$  or decrease in  $\alpha$ , while the resistance force,  $F_t$ , decreases with the increase in  $r_2$  or decrease in  $\alpha$ , and the reduction in  $F_t$  is greater than the increment in  $r$ , resulting in the decrease in the total resistance torque  $T$ . Thus, with a given maximum lockable load,  $F_{ml}$ , the required force,  $F_D$ , of the electromagnet can be reduced by increasing  $r_2$  and/or decreasing  $\alpha$ ; in other words, with a given output force,  $F_D$ , of the electromagnet, the maximum lockable load,  $F_{ml}$ , can be increased by increasing  $r_2$  and/or decreasing  $\alpha$ .

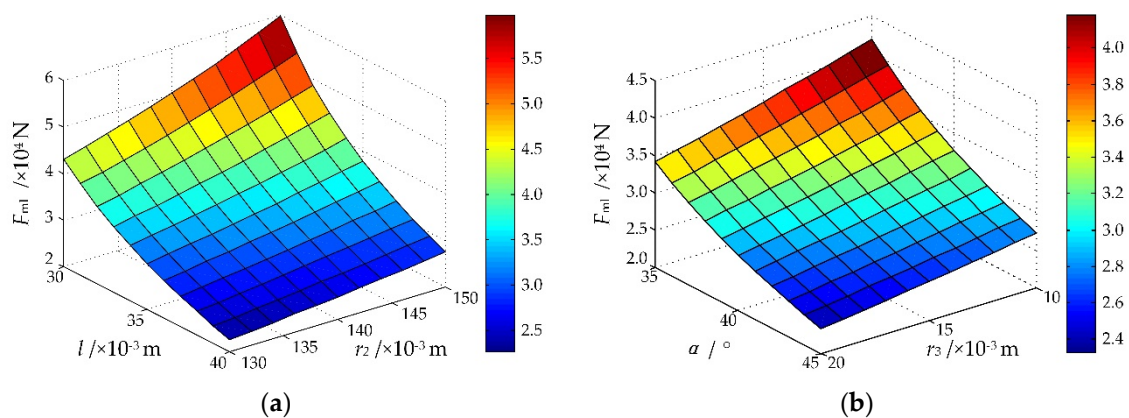
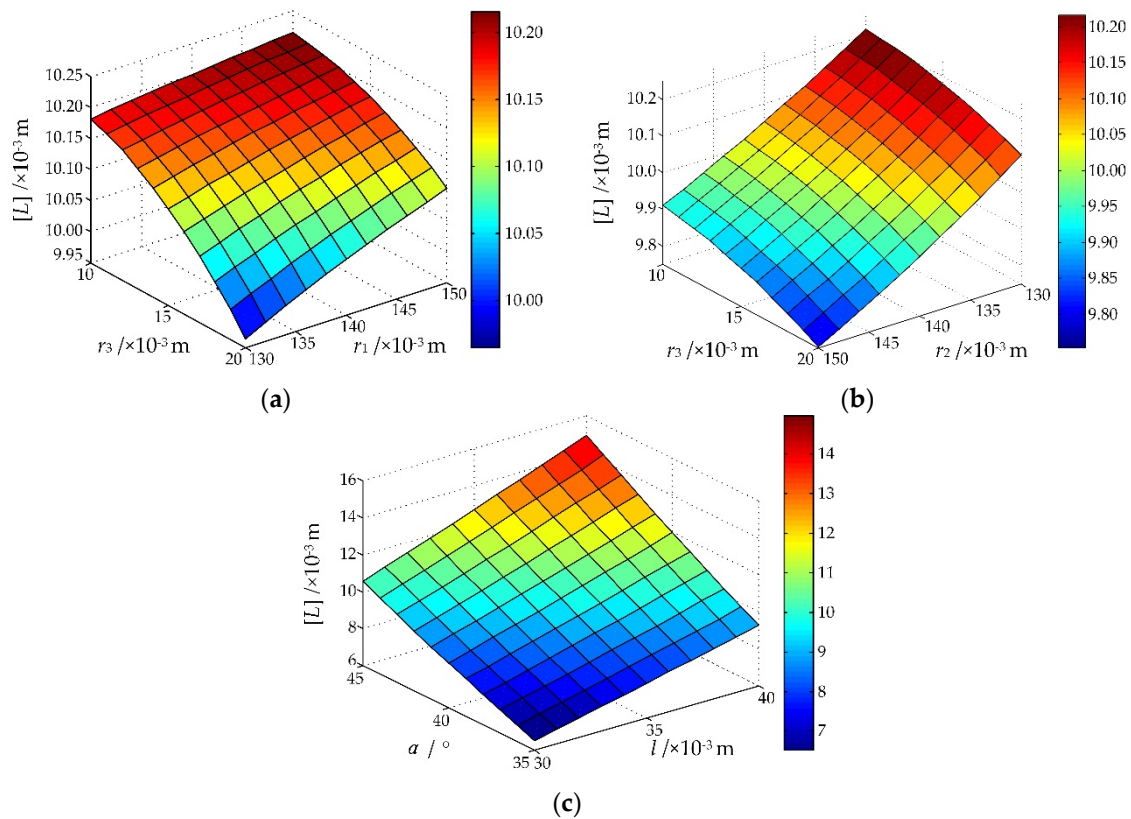


Figure 10. The lockable maximum load of the closing spring with (a) effects of  $r_2$  and  $l$ ; (b) effects of  $r_3$  and  $\alpha$ .

As shown in Figure 10,  $F_{ml}$  decreases with the increase in  $r_3$  and  $l$ . According to Equations (5), (10) and (11), both  $r$  and  $F_t$  increase with the increase in  $r_3$  and  $l$ , resulting in the increase in the total resistance torque  $T$ . Thus, with a given output force,  $F_D$ , of the electromagnet, the maximum lockable load,  $F_{ml}$ , can be decreased by increasing  $r_3$  and  $l$ .

Figure 11 shows the variable effects on the permissible stroke of the locking tab  $[L]$ .  $[L]$  increases with the increase in  $r_1$  and  $\alpha$  or decrease in  $r_3$ . The reason is that the angle of the notch of the locking ring,  $\delta$ , increases with the increase in  $r_1$  and  $\alpha$  or decrease in  $r_3$ , resulting in the rise of the rotation angle,  $\theta$ , of the locking ring in the locking or unlocking process. Thus  $[L]$  increases with the increase in  $r_1$  and  $\alpha$  or decrease in  $r_3$ .



**Figure 11.** The permissible stroke of the locking tab with (a) the effects of  $r_1$  and  $r_3$ ; (b) the effects of  $r_2$  and  $r_3$ ; (c) the effects of  $l$  and  $\alpha$ .

As shown in Figure 11,  $[L]$  can be decreased by increasing  $r_2$  and/or decreasing  $l$ . The reason is that as shown in Figure 9, the position of the contact point of the locking tab in the unlocking state, is not affected by the variation of  $r_2$  and  $l$ , while the position of the contact point of the locking tab in the locking state show upward tendency with the increase in  $r_2$  or decrease in  $l$ , resulting in the reduction in the relative position distance between the contact point in the locking state and that in the unlocking state. Thus  $[L]$  decreases with the increase in  $r_2$  or decrease in  $l$ .

#### 4.2. Sensitivity Analysis

Sensitivity is often used to evaluate the change of performance caused by a unit variable increment. The variable effects in Section 4.1 on the objective function can be quantified by the sensitivity. The sensitivity analysis of the lockable maximum load of the closing spring  $F_{ml}$  and the permissible stroke of the locking tab  $[L]$  is carried out in this section. Figures 12 and 13 show the sensitivities of  $F_{ml}$  and  $[L]$  with regard to the change rate of variables in the design space, respectively, with a sampling interval of 0.01% of the full range.

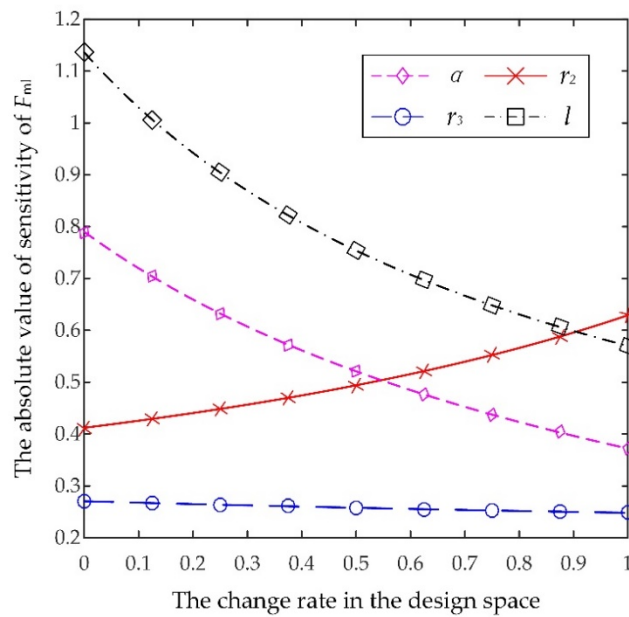


**Figure 12.** The absolute value of the sensitivities of  $F_{m1}$  with regard to the change rate of variables in the design space.

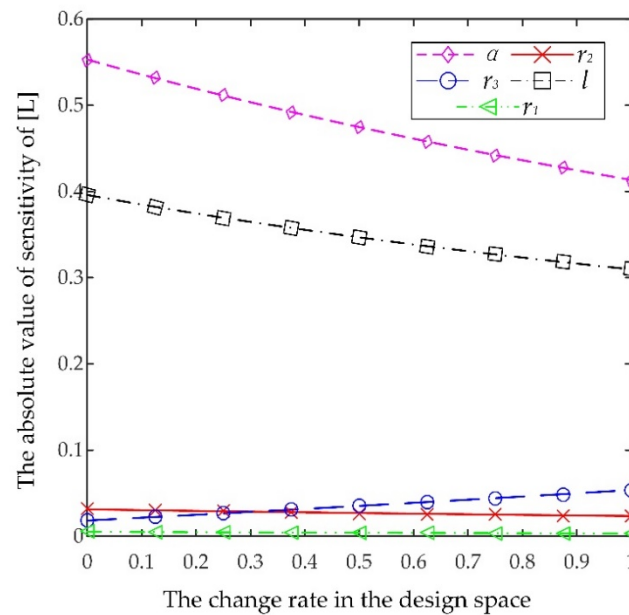


**Figure 13.** The absolute value of the sensitivities of  $[L]$  with regard to the change rate of variables in the design space.

As shown in Figure 12, the absolute value of the sensitivities of  $F_{m1}$  increases with the increase in  $r_2$ , and decreases with the increase in  $l$ ,  $\alpha$  and  $r_3$ . When the change rate ranges from 0% to 54.65%,  $l$  is the most sensitive variable and after that  $\alpha$ ,  $r_2$ ,  $r_3$ ; when the change rate ranges from 54.65% to 90.48%,  $l$  is still the most sensitive one and after that  $r_2$ ,  $\alpha$ ,  $r_3$ ; when the change rate ranges from 90.48% to 100%, the most sensitive variable is  $r_2$  and after that  $l$ ,  $\alpha$ ,  $r_3$ . The average variable sensitivities of  $F_{m1}$  are listed in Table 4. In the design space, the most sensitive variable of  $F_{m1}$  is  $l$  and after that  $\alpha$ ,  $r_2$  and  $r_3$ .

**Table 4.** The absolute values of the average variable sensitivities of  $F_{ml}$  in the design space.

| Design Variable Description  | Variable | Average Sensitivity |
|--|----------|---------------------|
| Radius of the notch of the locking ring  | $r_2$    | 0.5027              |
| Radius of the locking tab  | $r_3$    | 0.2583              |
| Center distance between the actuator working cavity and the locking ring notch | $l$      | 0.7852              |
| Radial deflection angle of the center of the locking ring notch                | $\alpha$ | 0.5403              |

As shown in Figure 13, the absolute value of the sensitivities of  $[L]$  increases with the increase in  $r_3$ , and decreases with the increase in  $r_2$ ,  $l$ , and  $\alpha$ ; the sensitivity of  $[L]$  to  $r_1$  remains on the lowest level in the full range;  $\alpha$  is the most sensitive variable in the full range and after that  $l$ ; when the change rate ranges from 0% to 30.63%,  $r_2$  is the third most sensitive variable and  $r_3$  is the fourth. The average variable sensitivities of  $[L]$  are listed in Table 5. In the design space, the most sensitive variable of  $[L]$  is  $\alpha$  and after that  $l$ ,  $r_3$ ,  $r_2$  and  $r_1$ .

**Table 5.** The absolute values of the average variable sensitivities of  $[L]$  in the design space.

| Design Variable Description  | Variable | Average Sensitivity |
|--|----------|---------------------|
| Radius of the actuator working cavity  | $r_1$    | 0.0042              |
| Radius of the notch of the locking ring  | $r_2$    | 0.0271              |
| Radius of the locking tab  | $r_3$    | 0.0355              |
| Center distance between the actuator working cavity and the locking ring notch | $l$      | 0.3488              |
| Radial deflection angle of the center of the locking ring notch                | $\alpha$ | 0.4775              |

#### 4.3. Analysis

According to the numerical analysis in Section 4.1, when  $r_1 = 150$  mm,  $r_2 = 150$  mm,  $r_3 = 10$  mm,  $l = 30$  mm and  $\alpha = 35^\circ$ , the lockable maximum load of the closing spring is  $F_{ml} = 109.414$  kN and the permissible stroke of the locking tab is  $[L] = 6.4059$  mm. However, the required working stroke of the locking tab  $L = 8$  mm  $> [L]$ , which means the above variable set cannot satisfy the requirement of the low-power holding mechanism. Thus, further optimization design is needed.

According to the sensitivity analysis in Section 4.2, in the design space of the low-power holding mechanism,  $[L]$  is more sensitive to  $l$  and  $\alpha$  rather than the other variables,  $r_1$ ,  $r_2$  and  $r_3$ . However,  $F_{ml}$  is also sensitive to  $l$ . So  $\alpha$  is the better option to be adjusted comparing with  $l$  to maximize the effect on the lockable maximum load of the closing spring. Through further numerical simulation, the improved parameter set of the low-power holding mechanism is obtained, as listed in Table 6, with the permissible stroke of the locking tab  $[L] = 8.0031$  mm, which satisfies  $[L] > L = 8$  mm, and the lockable maximum load of the closing spring is  $F_{ml} = 71.44$  kN after the parameter adjustment.

**Table 6.** The improved parameter set of the low-power holding mechanism.

| Parameter Description  | Symbol   | Optimal Solution |
|--|----------|------------------|
| Radius of the actuator working cavity  | $r_1$    | 150 mm           |
| Radius of the notch of the locking ring  | $r_2$    | 150 mm           |
| Radius of the locking tab  | $r_3$    | 10 mm            |
| Center distance between the actuator working cavity and the locking ring notch | $l$      | 30 mm            |
| Radial deflection angle of the center of the locking ring notch                | $\alpha$ | 39.31°           |

## 5. Conclusions

To bridge the gap of the low-power holding mechanism in the all-electric subsea gate valve actuator of the subsea production system, minimize the power consumption and cable number for



control and to improve the open-position keeping performance of all-electric subsea gate valve actuator, this paper proposed a novel low-power holding mechanism for the all-electric subsea gate valve actuator which can be applied to all-electric subsea gate valve actuators with various valve sizes and process pressure ratings. The paper also created mechanical and kinematic models, respectively, with regard to design variables, including the radius of the actuator working cavity  $r_1$ , the radius of the notch of the locking ring  $r_2$ , the radius of the locking tab  $r_3$ , the center distance between the actuator working cavity and the locking ring notch  $l$ , and the radial deflection angle of the center of the locking ring notch  $\alpha$ . Based on these analytic models, the variable effects on the lockable maximum load of the closing spring and the permissible stroke of the locking tab were analyzed. The parameter adjustment method was illustrated to satisfy the design criterion that the working stroke of the locking tab  $L$  should not exceed the permissible stroke of the locking tab  $[L]$ . The detailed conclusions are as follows:

- The proposed low-power holding mechanism is driven by the electromagnet and combines spiral transmission and cam-like transmission to convert the axial force of the closing spring into circumferential force to minimize the output force required as well as the number of the actuator's control cables, to improve the reliability and feasibility of the holding mechanism. The proposed low-power holding mechanism only requires a holding force of approximately 2%~7% of the maximum load of the closing spring to keep the valve open.
- With a given output force of the electromagnet, the lockable maximum load the low-power holding mechanism can be increased by increasing  $r_2$  or decreasing  $r_3$ ,  $l$  and  $\alpha$ . In the design space, the variable sensitivities of the lockable maximum load increases with the increase in  $r_2$  or the decrease in  $r_3$ ,  $l$  and  $\alpha$ ; the lockable maximum load is most sensitive to  $l$  and after that come  $\alpha$ ,  $r_2$  and  $r_3$  with regard to the average sensitivities in the design space.
- The permissible stroke of the locking tab increases with the increase in  $r_1$ ,  $l$  and  $\alpha$  or the decrease in  $r_2$  and  $r_3$ . In the design space, the variable sensitivities of the permissible stroke increase with the increase in  $r_3$  or the decrease in  $r_2$ ,  $l$  and  $\alpha$ ; the sensitivity of the permissible stroke to  $r_1$  remains on the lowest level in the full range; with regard to the average sensitivities of the permissible stroke, the most sensitive variable is  $\alpha$  and after that  $l$ ,  $r_3$ ,  $r_2$  and  $r_1$ .
- The design criterion is that the working stroke of the locking tab  $L$  should not exceed the permissible stroke of the locking tab  $[L]$ . The parameters can be adjusted to satisfy the criterion considering the variable sensitivities meanwhile minimizing the effect on the lockable maximum load. In the given case, the final parameter set of the low-power holding mechanism is:  $r_1 = 150$  mm,  $r_2 = 150$  mm,  $r_3 = 10$  mm,  $l = 30$  mm and  $\alpha = 39.31^\circ$ , with a lockable maximum load of the closing spring of 71.44 kN.

Further research will focus on the analysis of the influence of contact deformation and surface morphology on the modeling and the open-position keeping performance of the low-power holding mechanism. In addition, the future scope of the work can be directed toward the reliability assessment of the all-electric subsea gate valve actuator considering the subsea environment and the production fluid factors to ensure the long term application of the actuator in the subsea environment. The procedure in the paper can be applied to the design and research of other key components of the all-electric subsea production control system, such as the all-electric subsea ball valve actuator, which is required for the failsafe close ability and the open-position keeping function.

**Author Contributions:** Conceptualization, H.W. and P.J.; methodology, H.W. and L.W.; writing—original draft preparation, H.W., P.J. and L.W.; writing—review and editing, P.J., F.Y. and X.W.; visualization, G.W. and A.Z.; supervision, P.J., L.W. and A.Z.; funding acquisition, P.J., L.W., F.Y. and M.X. All authors have read and agreed to the published version of the manuscript.

**Funding:** This research was funded by the National Key Research and Development Program of China, grant number 2018YFC0310500; the High-Tech Ship Research Projects sponsored by the Ministry of Industry and Information Technology, grant number 2018GXB01; Fundamental Research Funds for the Central Universities, grant number 3072020CFT0702; the School Land Integration Development Project of Yantai (development and test platform of subsea production system), grant number 2019XDRHXMP29; China Postdoctoral Science Foundation,

grant number 2020M670889; National Natural Science Foundation of China, grant number 51779064; the Science and Technology Projects Sponsored by the West Coast of Qingdao New District, grant number 2019-157-2018-1-1.

**Conflicts of Interest:** The authors declare no conflict of interest.

## References

1. Winther-Larssen, E.; Massie, D.; Eriksson, K.G. Subsea all electric technology: Enabling next generation field development. In Proceedings of the Offshore Technology Conference, Houston, TX, USA, 2–5 May 2016. [\[CrossRef\]](#)
2. Wilson, A. All-electric subsea well brings benefits vs. traditional hydraulic technology. *J. Petrol. Technol.* **2018**, *70*, 65–66. [\[CrossRef\]](#)
3. Beckman, J. All-electric subsea controls strengthen security of K5 operations. *Offshore* **2008**, *68*, 42–44.
4. Akker, J.V.D.; Burdick, J. All-electric actuated subsea system qualified, implemented. *Oil Gas J.* **2008**, *106*, 44–50.
5. Akker, J.V.D.; Burdick, J. All-electric subsea production system brings advantages in ultra deepwater, long step-outs. *Offshore* **2008**, *68*, 136–141.
6. Abicht, D.; Akker, J.V.D. The 2nd generation DC all-electric subsea production control system. In Proceedings of the Offshore Technology Conference, Houston, TX, USA, 2–5 May 2011. [\[CrossRef\]](#)
7. Jia, Y.; Zhao, H. All-electric subsea production control system. *Appl. Mech. Mater.* **2013**, *251*, 196–200. [\[CrossRef\]](#)
8. Rokne, Ø. Deepwater developments can benefit from all-electric controls. *Offshore* **2013**, *7*, 108–109.
9. Schwerdtfeger, T.; Scott, B.; Akker, J.V.D. World-first all-electric subsea well. In Proceedings of the Offshore Technology Conference, Houston, TX, USA, 1–4 May 2017. [\[CrossRef\]](#)
10. Monteverde, C.; Novello, M.; Kristiansen, K. A new all electric subsea control system development. In Proceedings of the Offshore Technology Conference, Houston, TX, USA, 6–9 May 2019. [\[CrossRef\]](#)
11. Oh, J.S.; Kang, S.R. Merits of all-electric subsea production control system. *J. Korean Soc. Mar. Eng.* **2014**, *38*, 162–168. [\[CrossRef\]](#)
12. Fan, Y. Investigation of all-electric subsea control system. *Ocean Eng. Equip. Technol.* **2018**, *5*, 108–112. [\[CrossRef\]](#)
13. Abicht, D.; Halvorsen, G.R.; Ramberg, R.M. Subsea all-electric. In Proceedings of the Offshore Technology Conference, Houston, TX, USA, 1–4 May 2017. [\[CrossRef\]](#)
14. Pimentel, J.; Mackenzie, R.; Thibaut, E.; Garnaud, F. Seamlessly integrated subsea all-electric systems: Laggan-tormore as a case study. In Proceedings of the Offshore Technology Conference, Houston, TX, USA, 1–4 May 2017. [\[CrossRef\]](#)
15. Winther-Larssen, E.; Massie, D. All-electric as an enabler for more cost effective developments on cluster systems. In Proceedings of the Offshore Technology Conference, Houston, TX, USA, 1–4 May 2017. [\[CrossRef\]](#)
16. Orth, A.; Hendrix, G. An electro-mechanical actuator with hydrostatic drive for subsea trees to reduce CAPEX and OPEX with higher reliability and safety levels. In Proceedings of the Offshore Technology Conference, Houston, TX, USA, 30 April–3 May 2018. [\[CrossRef\]](#)
17. Elgsaas, K.M.; Hjertvikrem, T.; Hua, W.; Tryti, S.; Glomsaker, T. All-electric subsea systems—Intelligence on demand. In Proceedings of the Offshore Technology Conference, Houston, TX, USA, 30 April–3 May 2018. [\[CrossRef\]](#)
18. Elgsaas, K.M.; Hjertvikrem, T.; Hua, W.; Tryti, S.; Glomsaker, T. All-electric subsea systems deliver intelligence on demand: Data-driven approach to condition-based maintenance. *Offshore* **2018**, *78*, 43–47.
19. Hasan, Z.; Kapetanic, N.; Vaughan, J.; Robinson, G.M. Subsea field development optimization using all electric controls as an alternative to conventional electro-hydraulic. In Proceedings of the SPE/IATMI Asia Pacific Oil & Gas Conference and Exhibition, Nusa Dua, Bali, Indonesia, 20–22 October 2015. [\[CrossRef\]](#)
20. Zuo, X.; Yue, Y.; Duan, Y.; Guo, L. An overview of subsea production control system. *Ocean Eng. Equip. Technol.* **2016**, *3*, 58–66. [\[CrossRef\]](#)
21. Li, Z.; Jia, P.; Wang, H.; Zhang, N.; Wang, L. Development trend and active research areas of subsea production system. *J. Harbin Eng. Univ.* **2019**, *40*, 944–952. [\[CrossRef\]](#)
22. Xiao, X.; Zhao, H.; Wang, Y.; Peng, F.; Duan, M.; Yan, J.; Fan, X. Optimization design of coaxial parallel double spring of subsea valve actuator. *Oil Field Equip.* **2014**, *43*, 29–33. [\[CrossRef\]](#)

23. Yan, D.; Zhang, J.; Wang, P.; Feng, S. Design for a valve driver of subsea production system. *Machinery* **2017**, *55*, 13–15. [[CrossRef](#)]
24. Wang, X.; Liu, P.; Jia, P.; Zhang, L.; Wang, H.; Wang, S. Design of an all-electric subsea valve actuator and the strategy for multi-motor synchronous control. *China Offshore Oil Gas* **2017**, *29*, 149–156. [[CrossRef](#)]
25. Liu, P.; Liu, Y.; Wei, X.; Xin, C.; Sun, Q.; Wu, X. Performance analysis and optimal design based on dynamic characteristics for pressure compensated subsea all-electric valve actuator. *Ocean Eng.* **2019**, *191*, 106568. [[CrossRef](#)]
26. Winther-Larssen, E. Design of an Electric X-mas Tree Gate Valve Actuator. Master's Thesis, Norwegian University of Science and Technology, Trondheim, Norway, June 2007.
27. Berven, J. Subsea Production Control Systems for All-Electric X-mas Trees. Master's Thesis, University of Stavanger, Stavanger, Norway, June 2013.
28. Xiao, Y.; Wu, D.; Xiang, C.; Li, S. Design of production gate valve and actuator for subsea all-electric Christmas tree. *China Petrol. Mach.* **2018**, *46*, 60–64. [[CrossRef](#)]
29. Tareen, W.U.; Mekhilef, S. Transformer-less 3P3W SAPF (three-phase three-wire shunt active power filter) with line-interactive UPS (uninterruptible power supply) and battery energy storage stage. *Energy* **2016**, *109*, 525–536. [[CrossRef](#)]
30. Stropnik, R.; Sekavčnik, M.; Ferriz, A.M.; Mori, M. Reducing environmental impacts of the ups system based on PEM fuel cell with circular economy. *Energy* **2018**, *165*, 824–835. [[CrossRef](#)]



© 2020 by the authors. Licensee MDPI, Basel, Switzerland. This article is an open access article distributed under the terms and conditions of the Creative Commons Attribution (CC BY) license (<http://creativecommons.org/licenses/by/4.0/>).